World Conference on Timber Engineering Oslo 2023

AN ACCURATE FINITE ELEMENT MODEL TO STUDY THE PROGRESSIVE COLLAPSE OF POST-AND-BEAM MASS TIMBER BUILDINGS

Chunhao Lyu[1], Benoit P. Gilbert[2], Hong Guan[3], Hassan Karampour[4], Shanmuganathan Gunalan[5], William Leggate[6]

ABSTRACT: The structural behaviour of mass timber buildings under the removal of a load bearing element is complex. To well understand this phenomenon and ultimately develop scientifically based design guidelines against progressive collapse for this type of buildings, there is a need to develop Finite Element models which accurately capture the non-linear structural responses of such buildings. This paper presents how mass timber post-and-beam systems can be accurately modelled using Finite Element under edge and corner column removal scenarios. The model was validated against published 3D experimental tests performed on scaled-down substructures. Results show that the model accurately replicated non-linear behaviour, load redistribution mechanisms, ultimate loads, failure modes, and strain developments. The use of the model was then illustrated by running parametric studies to quantify (i) the influence of the Cross Laminated Timber (CLT) floor panels layout and (ii) one alternative load path, typically ignored in design, on the progressive collapse resistance capacity.

KEYWORDS: Numerical simulations, Finite element, Mass timber post-and-beam buildings, Progressive collapse, Disproportionate collapse, Floor CLT panels layout

1 INTRODUCTION

Progressive collapses of buildings are triggered by abnormal loads, such as explosions, vehicle impacts, construction and design errors, fire and natural disasters [1]. These loads induce a local damage which may propagate throughout the building in a chain reaction, leading to its partial or entire collapse [2, 3]. While these events are rare, they result in significant economic losses, especially for tall buildings, and potential human casualties.

Mid-rise to tall mass timber buildings, i.e. buildings assembled from engineered wood products, such as Laminated Veneer Lumber (LVL), Glued laminated timber (Glulam) and Cross Laminated Timber (CLT) [4], are increasingly gaining international popularity. As these buildings become taller, commonly reaching six storeys and more, the consequences of a potential progressive collapse event also significantly increase. Studying the progressive collapse of mass timber buildings is still a relatively new research topic, and the structural response of various types of mass timber buildings to resist such events has been researched so far, through experimental [5-9], analytical [10, 11] or numerical [12-15] methods. However, the accuracy of the developed numerical models has not yet been verified against experimental tests, or only on component tests [15]. To improve design guidelines, such as the US Department of Defence (DoD) [16], the General Services Administration (GSA) [17], the Institution of Structural Engineers (IStructE) [18] and WoodSolutions technical guides [19, 20], there is a need to develop Finite Element (FE) models which are proven to accurately replicate the structural behaviour of mass timber buildings under a load bearing element removal scenario. Such FE models have been widely used in reinforced concrete and steel structural systems [21-28] to gain in-depth understanding on the structural behaviour through parametric studies and identify the key factors affecting the ability of the structures to resist progressive collapse. Mass timber buildings differ from their concrete [29-32], steel [33-35] and composite-steel [36, 37] counterparts, due to the lack of structural continuity (as built from prefabricated structural elements), the brittle failure mode of the material [38], and the typical lack of ductility of timber-to-timber connections [6, 39]. These characteristics result in mass timber buildings deemed to have fewer possibilities to redistribute the load after the loss of a load bearing elements [19], outlining the necessity to develop an accurate model specific to mass timber buildings.

Consequently, this paper presents how post-and-beam mass timber buildings can be accurately modelled using FE. The proposed numerical model was validated herein against quasi-static 3D experimental tests, performed by

[1] Chunhao Lyu, Griffith University, Australia, c.lyu@griffith.edu.au
[2] Benoit P. Gilbert, Griffith University, Australia, b.gilbert@griffith.edu.au
[3] Hong Guan, Griffith University, Australia, h.guan@griffith.edu.au
[4] Hassan Karampour, Griffith University, Australia, h.karampour@griffith.edu.au
[5] Shanmuganathan Gunalan, Griffith University, Australia, shanmuganathanguna.gunalan@griffith.edu.au
[6] William Leggate, Griffith University, Australia, william.leggate@griffithuni.edu.au

https://doi.org/10.52202/069179-0368

the authors, on scaled-down substructures subjected to edge and corner column removal scenarios, totalling three different tests [7, 8]. As the layout of the CLT floor panels plays a critical role in redistributing the load through the building [7, 8], the influence of various CLT floor panels layouts on the progressive collapse resistance was numerically investigated through parametric study. The influence of the beam-to-column connections of the beams connected to the removed column on the ability of the building to redistribute the load was also studied.

2 FE MODEL OF 3D TESTS

2.1 GENERAL

The commercial finite element software package ABAQUS 6.14 [40] was used to simulate the 3D experimental tests. The beams and columns were modelled using beam elements B31. The 3-ply CLT panels were modelled using four-node general-purpose layered shell elements S4R. The *Composite Layup* tool was employed to define the material properties, thickness and orientation of each ply. Specifically, two types of *Lamina* materials were defined based on the properties provided by the manufacturer [41], namely 20 mm thick external (referred to as "*G8*") and 35 mm thick internal (referred to as "*G6*") laminae. A transversely isotropic material was used for each lamina, with the inputted longitudinal (*L* – parallel to the grain) and transverse (*T* – perpendicular to the grain) material properties summarised in Table 1. The two outer laminae were parallel to the face boards direction while the middle lamina was perpendicular to the two outer laminae. All connector properties were obtained from testing individual components and detailed in [42].

Table 1: *Material properties used in the numerical simulation*

Element	Moduli of Elasticity		Poison ratio	Shear moduli	
	E_L (MPa)	E_T (MPa)	μ_{LT} (-)	G_{LT} (MPa)	G_{TT} (MPa)
Beam/Column	14,100	-	-	800	-
CLT (outside layers)	9,000	450	0.3	700	90
CLT (inside layer)	6,000	300	0.3	400	60

Note: $_L$ – Longitudinal, parallel to the grain direction
$_T$ – Transverse, perpendicular to the grain direction (i.e., in both tangential and radial directions)

2.2 LOADING TREE

The two triangular steel plates and the six rectangular loading pads of the six-point loading tree (see [7] for more details) were simulated with four-node general-purpose shell elements S4R. The spreader beam linking the two plates was modelled with first-order beam elements B31. All these elements were assigned rigid material properties. Three-dimensional CONN3D2 connector elements were employed to connect the different elements together. The detailed model and the connector properties are shown in Figure 1. This model enabled the loading tree it to freely deform without resisting the applied load as in [7, 8]. The four corner nodes of each loading pad were connected to the CLT panels with only the translations restrained, the elements were therefore free to rotate relative to each other. Additionally, the contact between the six rectangular loading pads and the CLT panels was simulated using the "*hard contact* + *Rough*" surface-to-surface contact property, enabling pressure transmission without penetration in the normal direction and no sliding in the tangential directions.

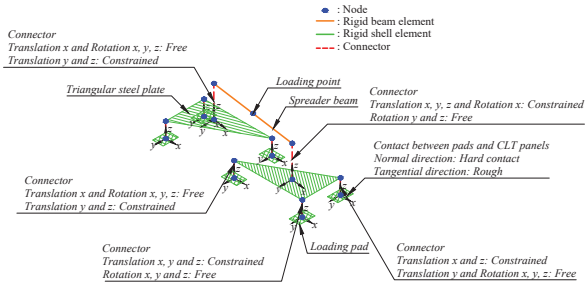

Figure 1: *Six-point loading tree details with local coordinate systems*
(Note: (i) connectors have a nil length in the model but are shown apart in the figure to clarify; (ii) the connector properties shown for the right triangular plate also apply to the left plate)

2.3 BOUNDARY CONDITIONS AND APPLIED LOADS

The overview of the FE model simulating Test EM-1 (and its repeat Test EM-2), with the boundary conditions, is shown in Figure 2. In reference to the global coordinate system *X*-*Y*-*Z*, the displacements of the bottom node of the eight permanent columns were restrained along all axes, while all rotations were released. To simulate the horizontal restraints provided to the substructure (See [7]): (i) the displacement along the *X*-axis of the six peripheral columns shown in Figure 2 was restrained at the elevation of the centreline of the beams and (ii) the edge nodes of the CLT panels shown in Figure 2 had their displacement along the *Z*-axis restrained. The same principles applied to Tests CM-1 and CM-2, but with the locations of the horizontal restraints given in [8].
In the analyses, the same loading sequence as in [7, 8] was simulated and consisted of:

- *Step 1:* Applying the self-weight of (i) the CLT panels of 0.37 kPa (average measured value on 27 panels) as an UDP, (ii) the weights, loaded on the bays not adjacent to the removed column, of 4.8 kPa as an UDP, and (iii) the loading tree (weighing 10.3 kN for Tests EM-1 and EM-2, and 9.4 kN for Tests CM-1 and CM-2) as a point load applied at mid-span of the spreader beam of the tree (see Figure 1). Note that the bottom node of the column stub of the removed column was constrained in displacement along the three degrees of freedom to simulate an undamaged structure during this step.
- *Step 2:* Removing the boundary conditions at the bottom node of the removed column.
- *Step 3:* Displacing along the negative *Y*-axis the node at mid-span of the spreader beam of the loading tree (see Figure 1) to simulate the applied load, maintaining the load applied in *Step 1*.

https://doi.org/10.52202/069179-0368

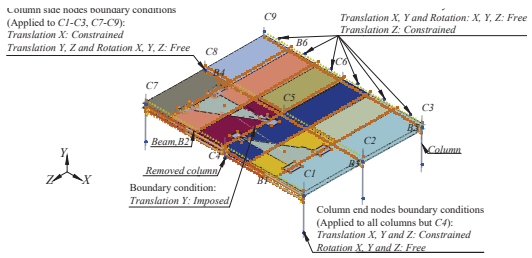

Figure 2: *Numerical model overview with boundary conditions shown for Test EM-1*

2.4 CONNECTIONS AND TIMBER FAILURE MODELLING

Connector elements CONN3D2, with the connector type *"Cartesian + Rotation"*, i.e., allowing all degrees of freedom to be entered by the user, were employed to connect the different components of the structure together, as described in [42].

Bending failure of the beams was observed experimentally in [7, 8] and while the beams were modelled elastically, bending failure of the beams was included in the model with connectors, used as fuses. The region of the maximum bending moment of the critical beams, i.e., the mid-span region of the middle row of beams, was modelled in 10 beam elements of 100 mm each. Adjacent segments were connected together by rigid connectors of zero length, therefore not affecting the elastic mechanical behaviour of the beams. The "*failure*" criteria option was used in the connectors to release the rotational stiffness when the bending moment reached the experimentally measured moment capacity of 13.7 kNm [7], therefore simulating the bending failure. The principle is illustrated in Figure 3 and was found (not shown herein) to correctly model the bending failure of the beams.

As the failure of the CLT panels was not explicitly observed experimentally, failure of the CLT panels was not modelled.

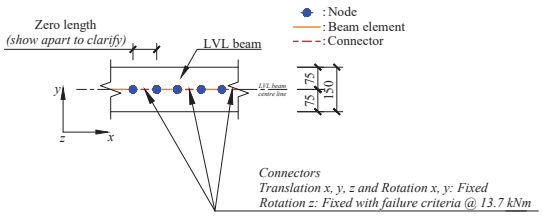

Figure 3: *Modelling bending failure of LVL beams (unit: mm)*

3 3D MODEL VALIDATION

3.1 LOAD-DISPLACEMENT CURVES AND FAILURE MODES

Figure 4 compares the experimental and numerical applied load in *Step 3* (see Section 2.3) versus the removed column displacement, under an edge column removal scenario. Note that the weight of the loading tree was included in the figure by offsetting the curves along the vertical axis as in [7]. Two numerical simulations were run with the shear capacity of the beam-to-column connections either inputted from the values obtained with or without the CLT panels, as discussed in [42]. Ignoring the contribution of the CLT panels in the shear capacity of the beam-to-column connections resulted in the FE analysis underestimating the ultimate load by 26% due to the premature failure of these connections in the second row of beams. It is therefore important to consider this contribution to accurately reproduce the overall structural behaviour and is now considered in this study.

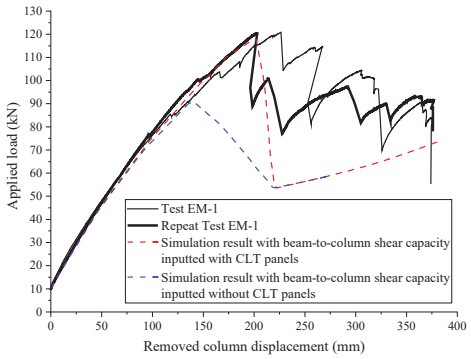

Figure 4: *Load – displacement curves from tests and numerical simulations (Edge column removal scenario only)*

Table 2 compares the experimental and numerical initial stiffness and ultimate loads for the edge column removal scenarios. The FE model accurately (within 3%) replicated both the initial stiffness and ultimate load.

Table 2: *3D FEA results comparison*

Specimen	Initial stiffness (kN/mm)			Ultimate load (kN)		
	Test	FE	Test/FE	Test	FE	Test/FE
EM-1	0.61	0.64	0.95	120.8	118.0	1.02
EM-2	0.66		1.03	120.4		1.02
CM-1	0.21	0.22	0.95	59.9	68.3	0.88
CM-2	0.75	0.63	1.19	97.3	105.7	0.92
		Average	1.03		Average	0.96
		COV	11%		COV	8%

In terms of failure modes, the FE model predicted shear failure to occur at the beam-to-column connectors linking both beams *B3* and *B4* to the interior column *C5* (see Figure 2 for element numbering). This failure mode corresponds well to the one experimentally observed for which shear failure occurred at beam *B3*-to-column *C5* connection. The difference of having two connections failing numerically, when compared to one connection failing experimentally, can be explained by the variability in the connection capacity. As the two connections are loaded similarly and have the same numerical capacity, they fail at the same time in the FE model. Experimentally, one connection will be statistically stronger that the other one, fail first and allow the load to redistribute before the second connection fails.

Note that the maximum load was reached due to bending failure of beam *B4* when repeating Test EM-1 (dotted line in Figure 4). This failure mode was also observed in Test EM-1 but after shear failure of the connection occurred. Bending failure was not observed numerically due to the

https://doi.org/10.52202/069179-0368

connections failing first in shear, and consequently unloading the beams due to the total applied force dropping.

Figure 5 plots the applied load versus the removed column displacement under the two different corner column removal scenarios. Regarding Test CM-1, the initial stiffness matched well with the experimental test, and the predicted ultimate load was 14.0% higher than the experimental test. The beam *B4* bending failure, which was predicted in the FE model was also observed in the experimental test. In the simulation, after the load dropped due to bending failure of beam *B4*, the load steadily increased, likely because the interaction between the bending moment and shear force in the behaviour of the beam-to-column connectors was not considered. Indeed, this allowed the applied load to be fully transferred to columns *C4* and *C8* in shear through the beam-to-column connectors, despite these connections completely failing in bending and likely having a reduced shear capacity. Also see Section 3.2 on the load transfer.

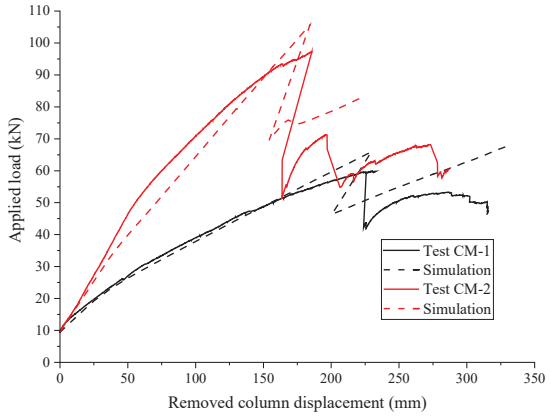

Figure 5: *Load – displacement curves from tests and numerical simulations (Corner column removal scenario only)*

For Test CM-2, the initial stiffness was 20% different between the experimental test and the simulation results, but the overall trend of the load-displacement curve was well captured. Regarding the ultimate load, the experimental and numerical ratio was equal to 0.92. The FE model predicted failure to occur in bending at beam *B3*, matching well with the failure observed in Test CM-2. The numerical model stopped when the removed column displacement reached 220 mm, corresponding to the beam-to-column connector linking beam *B3* and column *C2* reaching its ultimate bending capacity.

3.2 LOAD REDISTRIBUTION

Figure 6 compares the experimental and numerical load redistribution through the system, taken as the column reaction forces, versus the removed column displacement. As the results for Test EM-1 and its repeat Test EM-2 were similar [7], only the results from Test EM-1 are plotted in the figure for clarity. The figure shows that up to reaching the ultimate load, corresponding to a removed column displacement of 122 mm, the numerical model accurately reproduced the load redistribution through the system. After failure, the numerical column reaction force for column *C5* dropped significantly more than the experimental tests due to the two beam-to-column connectors at column *C5* failing numerically against only one experimentally. The load redistribution after failure was however correctly captured for all other columns.

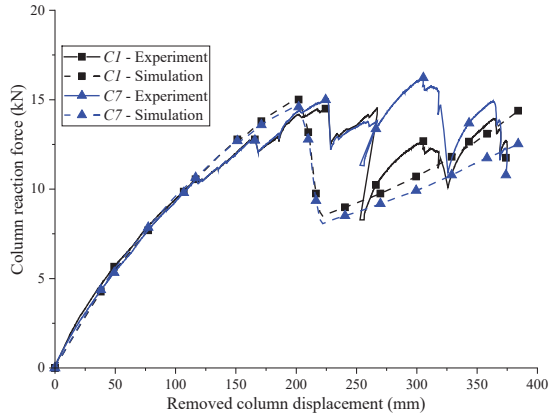

(a) Adjacent columns to removed column

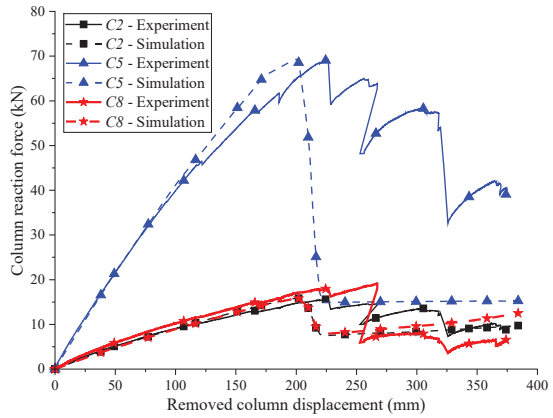

(b) Interior and 2nd-row side columns

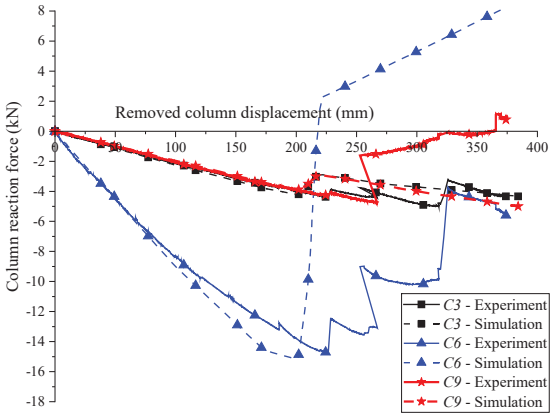

(c) 3rd-row column (back row)

Figure 6: *Load redistribution for edge column removal scenario (shown for Test EM-1)*

Figure 7 plots the experimental and numerical column reaction forces versus the removed column displacement for Test CM-1. Overall, the load redistribution was predicted well for all columns as outlined in the figure. The column reaction forces from Test CM-2 and simulation results are now compared in Figure 8. Similarly to the other two tests, the load redistribution was well captured by the numerical model for Test CM-2.

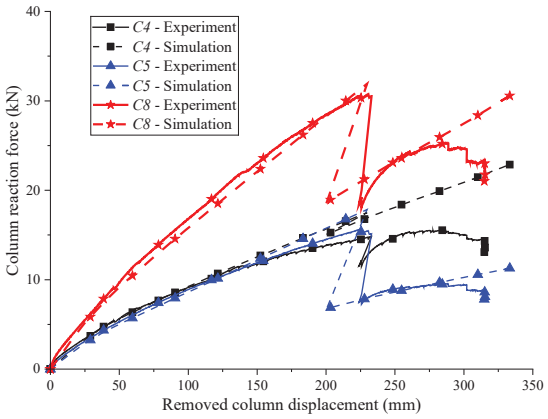

(a) Adjacent columns to removed column and interior column

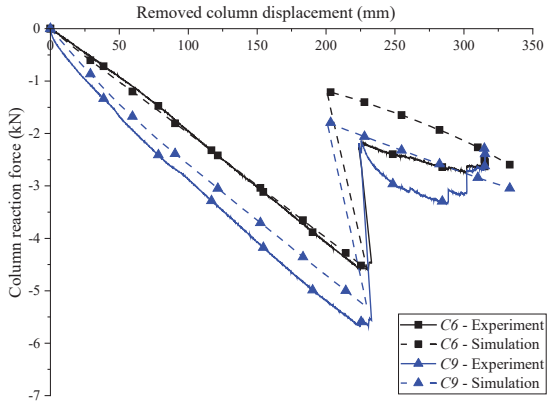

(b) 3rd-row columns (back row)

***Figure 7:** Load redistribution for corner column removal scenario (shown for Test CM-1)*

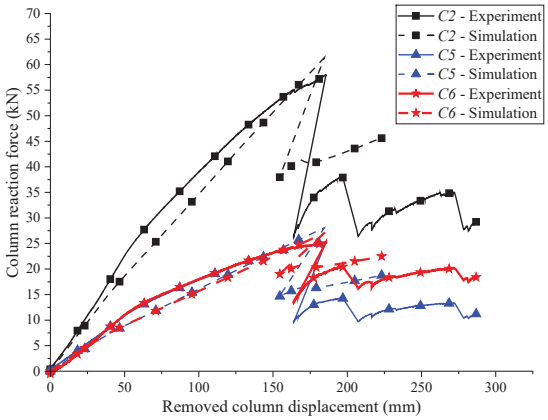

(a) Adjacent columns to removed column and interior column

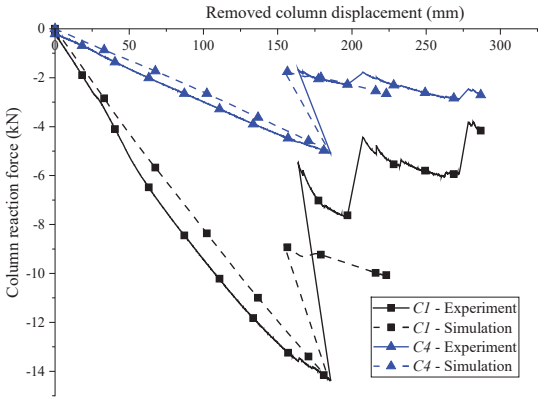

(b) 1st-row columns (front row)

***Figure 8:** Load redistribution for corner column removal scenario (shown for Test CM-2)*

4 PARAMETRIC STUDIES

The validated 3D numerical models are used in this section to perform parametric studies by evaluating the influence of (i) the CLT floor panels layout and (ii) one alternative load path typically not considered in design, on the ability of the building to resisting progressive collapse. In total, eleven additional models were run as part of this section.

4.1 INFLUENCE OF VARIOUS CLT PANEL LAYOUTS

To cover different design practices than the staggered CLT panels from the validated model in Section 3, two additional layouts of the CLT floor panels were considered in this section. In the first and second additional layouts, all floor panels spanned one and two bays, respectively. Analyses were run for both edge and corner columns removal scenarios.

4.1.1 Edge Column Removal Scenario

Figure 9 (a) compares the numerical applied loads in *Step 3* (see Section 2.3) versus the removed edge column displacement for the three different layouts of the CLT panels. Results showed that the initial stiffness was significantly influenced by the CLT panel layouts, with the stiffness when all panels spanned two bays being 4.6 times greater than when all panels spanned one bay. However, the capacity of the staggered and all two-bay long panels was within 3.5% of each other. The failure mode for these two configurations was the shear failure of the beam-to-column connectors on both side of interior column *C5*. For the all one-bay long panels, no specific failure mode was numerically observed. All configurations allowed to withstand an accidental design load of 8.95 kPa in the DoD [16], i.e. corresponding to an applied load of 53.7 kN.

4.1.2 Corner Column Removal Scenario

Figure 9 (b) compares the numerical applied load in *Step 3* versus the removed column displacement for the four

https://doi.org/10.52202/069179-0368

panel layouts, i.e., staggered (Tests CM-1 and CM-2), all two-bay long panels and all one-bay long panels. The initial stiffness of the all two-bay long panels was similar to the one of simulated Test CM-2. However, and while the same failure mode was encountered for these two layouts (i.e., bending failure of beam *B4*), due to different load distributions of the beam, the ultimate load of the all two-bay long panels was 10% lower. Similar to the edge column removal scenario, the model for all one-bay long panels showed the lowest initial stiffness and no specific failure mode was numerically observed. All configurations allowed to withstand an accidental design load of 8.95 kPa in the DoD [16], i.e. corresponding to an applied load of 26.9 kN.

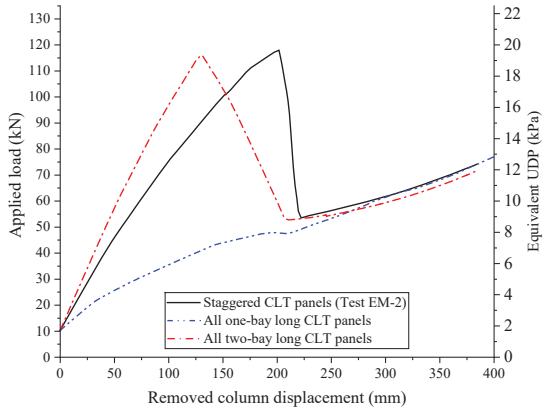

(a) Edge column removal scenario

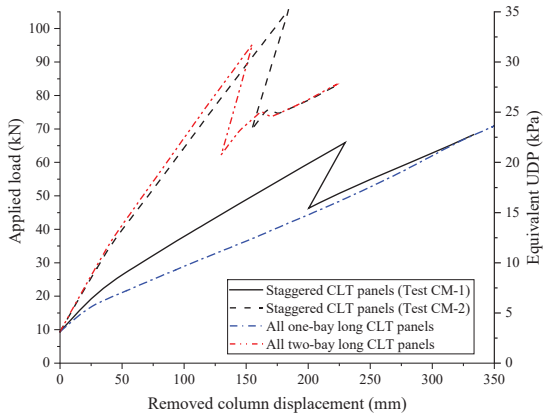

(b) Corner column removal scenario

Figure 9: *Numerical applied force versus removed column displacement for different CLT panel layouts*

4.2 INFLUENCE OF THE BEAM-TO-COLUMN CONNECTORS OF THE FRONT FRAME

During the experimental investigations [7, 8], and as captured by the previous numerical investigations, the beam-to-column connections of the beams connected to the removed column, but located at the opposite end of this column, provided a local support to the CLT panels above. This alternate load path allowed to transfer about 29% of the applied load to the columns directly connected to the removed one by these beams [7]. This local support can be seen in Figure 6 (a), Figure 7 (a) and Figure 8 (a), in which despite experiencing large rotation, the beam-to-column connections did not fail in shear and transferred load to the columns adjacent to the removed one. However, in a design situation and as no data would typically be available on the shear capacity of the beam-to-column connections experiencing large rotation, this alternative load path would be ignored. In other words, all beam-to-column connections of the beams attached to the removed column would be assumed to have failed and not carrying load.

To investigate the influence and the importance of the alternate load path mentioned above to the response of the building, another seven models were analysed with the same CLT layouts as in Section 4.1. In these models, (i) under the edge column removal scenario, the beam-to-column connectors of both beams *B1* and *B2* were ignored and removed from the models, and (ii) for the corner column removal scenario, the beam-to-column connectors of both beams *B2* and *BP3* were similarly removed from the models. The results, in terms of applied load versus removed column displacement, are plotted in Figure 10.

For the model with all one-bay long panels and edge column removal scenario, the structure was not able to carry its self-weight and loading tree when removing the column in *Step* 2 (see Section 2.3), so the response was not plotted in Figure 10 (a). This result shows the importance of the alternative load path offered by the beam-to-column connectors providing local support to the CLT panels above.

Still for the edge column removal scenario, the maximum load was reached for both staggered and two-bay long panels due to shear failure of the beam-to-column connectors linking beams *B3* and *B4* to column *C5*. The former and latter layouts reached a capacity 8.5 and 10.7 times higher, respectively, than the accidental design load of 8.95 kPa in the DoD [16]. In both scenarios, the models were not able to converge after the shear failure of the connectors, due to the sharp decrease of the load.

For the corner column removal scenario, the layout corresponding to one-bay long panels did not reached the accidental design load of 8.95 kPa in the DoD [16], while all other configurations reached a capacity at least 2.2 times greater than this accidental design load.

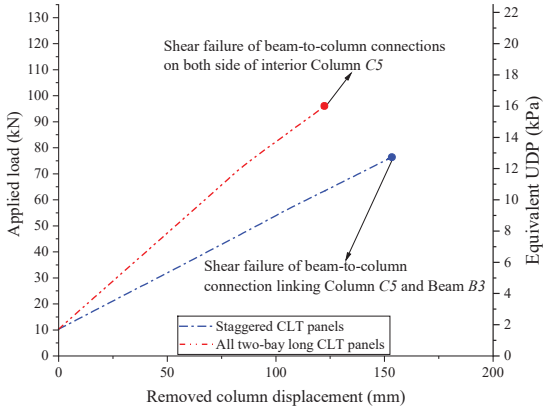

(a) Edge column removal scenario

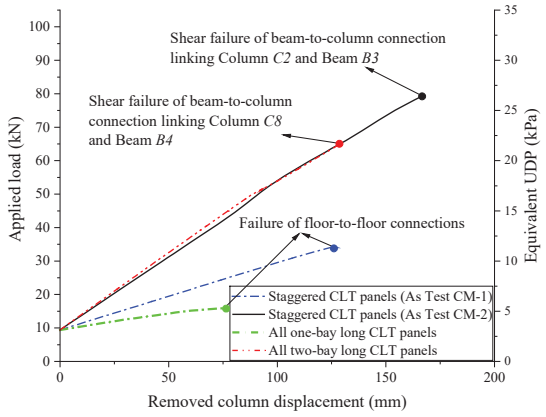

(b) Corner column removal scenario

Figure 10: *Numerical applied force versus removed column displacement when ignoring the beam-to-column connectors linked to the removed column*

5 CONCLUSIONS

This paper presented and validated FE models of post-and-beam mass timber buildings under various column removal scenarios. Parametric studies using the validated numerical model were conducted. The main conclusions of this paper can be summarised as follow:

1. The FE model of the 3D substructures was found to accurately replicate the experimentally observed ultimate loads, initial stiffness, failure modes, load redistributions, deformed shapes and strain developments. The experimental-to-numerical initial stiffness and ultimate load were 1.03 and 0.96, respectively, with associated coefficients of variation less than 0.11.
2. When performing component tests, it was found that the CLT panels could significantly influence the shear capacity of the beam-to-column connections by delaying the failure. An increase in 30% in the shear capacity was attributed to the presence of the CLT panels. This behaviour needs to be considered to accurately capture the structural behaviour of post-and-beam mass timber buildings.
3. Parametric studies showed that if two-bay CLT panels are used: (i) for an edge column removal scenario, staggering or not does not influence the ultimate load, however, (ii) for a corner removal scenario, staggering the panels was found to influence the ultimate by up to 60.3%, when compared to non-staggered panels.
4. Parametric studies also showed that the alternative load path providing by the beam-to-column connectors of the frames connected to the removed column, and locally supporting the CLT panel above, is essential to achieve robustness when only one-bay long CLT panels are used. If this alternative load path cannot be relied on, post-and-beam mass timber buildings with one-bay long CLT panels are not able to resist the accidental design load under a column removal scenario.
5. The validated model can be used to eventually (i) quantify all parameters influencing the behaviour of post-and-beam mass timber buildings to resist progressive collapse, (ii) characterise the properties of timber-to-timber connections required to ensure robustness, (iii) evaluate the alternative load paths in an entire building and (iv) provide data to develop design guidelines.

ACKNOWLEDGEMENT

This study was funded by the School of Engineering and Built Environment, the Griffith University Sciences group and the Australian Research Council (ARC) Industrial Transformation Research Hub IH150100030 on tall timber buildings.

REFERENCES

[1] Adam, J. M., Parisi, F., Sagaseta, J., Lu, X.: Research and practice on progressive collapse and robustness of building structures in the 21st century. Engineering Structures, 173:122–149, 2018.

[2] Ellingwood, B. R.: Mitigating risk from abnormal loads and progressive collapse. Journal of Performance of Constructed Facilities, 20(4):315–323, 2006.

[3] American Society of Civil Engineers, Minimum design loads for buildings and other structures, *(ASCE/SEI 7–10)*, 2013.

[4] Connolly, T., Loss, C., Iqbal, A., Tannert, T.: Feasibility study of mass–timber cores for the UBC tall wood building. Buildings, 8(8), 2018.

[5] Mpidi Bita, H., Tannert, T.: Experimental study of disproportionate collapse prevention mechanisms for mass–timber floor systems. Journal of Structural Engineering, 146(2):04019199, 2020.

[6] Lyu, C. H., Gilbert, B. P., Guan, H., Underhill, I. D., Gunalan, S., Karampour, H., Masaeli, M.: Experimental collapse response of post-and-beam mass timber frames under a quasi-static column removal scenario. Engineering Structures, 213:110562, 2020.

[7] Lyu, C. H., Gilbert, B. P., Guan, H., Underhill, I. D., Gunalan, S., Karampour, H.: Experimental study on the quasi-static progressive collapse response of post-and-beam mass timber buildings under an edge column removal scenario. Engineering Structures, 228:111425, 2021.

[8] Lyu, C. H., Gilbert, B. P., Guan, H., Underhill, I. D., Gunalan, S., Karampour, H.: Experimental study on the quasi-static progressive collapse response of post-and-beam mass timber buildings under corner column removal scenarios. Engineering Structures, 242:112497, 2021.

[9] Cheng, X., Gilbert, B. P., Guan, H., Underhill, I. D., Karampour, H.: Experimental dynamic collapse response of post–and–beam mass timber frames under a sudden column removal scenario. Engineering Structures, 233:111918, 2021.

[10] Mpidi Bita, H., Tannert, T.: Tie-force procedure for disproportionate collapse prevention of CLT

https://doi.org/10.52202/069179-0368

platform–type construction. Engineering Structures, 189:195–205, 2019.
[11] Voulpiotis, K., Köhler, J., Jockwer, R., Frangi, A.: A holistic framework for designing for structural robustness in tall timber buildings. Engineering Structures, 227:111432, 2021.
[12] Mpidi Bita, H., Currie, N., Tannert, T.: Disproportionate collapse analysis of mid–rise cross–laminated timber buildings. Structure and Infrastructure Engineering, 14(11):1547–1560, 2018.
[13] Mpidi Bita, H., Tannert, T.: Disproportionate collapse prevention analysis for a mid–rise flat–plate cross–laminated timber building. Engineering Structures, 178:460–471, 2019.
[14] Huber, J. A. J., Ekevad, M., Girhammar, U. A., Berg, S.: Finite element analysis of alternative load paths in a platform–framed CLT building. Proceedings of the Institution of Civil Engineers: Structures and Buildings, 173(5):379–390, 2020.
[15] Huber, J. A. J., Mpidi Bita, H., Tannert, T., Berg, S.: Finite element analysis of alternative load paths to prevent disproportionate collapse in platform-type CLT floor systems. Engineering Structures, 240:112362, 2021.
[16] Department of Defence, Design of buildings to resist progressive collapse *(UFC 4–023–03)*, 2016.
[17] General Services Administration, Alternate path analysis and design guidelines for progressive collapse resistance, Washington, DC: General Services Administration, 2016.
[18] Institution of Structural Engineers, Practical guide to structural robustness and disproportionate collapse in buildings, London, UK. Institution of Structural Engineers Limited, 2010.
[19] Hewson, N., Technical design guide #39: Robustness in structures, Melbourne, VIC. Forest & Wood Products Australia Limited, 2016.
[20] Woodard, A., Jones, A., Technical design guide #50: Mid–rise timber building structural engineering, Melbourne, VIC. Forest & Wood Products Australia Limited, 2019.
[21] Bao, Y., Kunnath, S. K., El-Tawil, S., Lew, H. S.: Macromodel-based simulation of progressive collapse: RC frame structures. Journal of Structural Engineering, 134(7):1079–1091, 2008.
[22] Han, Q., Li, X., Liu, M., Spencer, B. F.: Performance analysis and macromodel simulation of steel frame structures with beam-column joints using cast steel stiffeners for progressive collapse prevention. Thin–Walled Structures, 140:404–415, 2019.
[23] Khandelwal, K., El-Tawil, S., Kunnath, S. K., Lew, H. S.: Macromodel–based simulation of progressive collapse: Steel frame structures. Journal of Structural Engineering, 134(7):1070–1078, 2008.
[24] Yang, B., Tan, K. H.: Robustness of bolted–angle connections against progressive collapse: Experimental tests of beam–column joints and development of component–based models. Journal of Structural Engineering, 139(9):1498–1514, 2013.
[25] Fu, Q., Tan, K. H., Zhou, X. H., Yang, B.: Numerical simulations on three-dimensional composite structural systems against progressive collapse. Journal of Constructional Steel Research, 135:125–136, 2017.
[26] Kunnath, S. K., Bao, Y., El-Tawil, S.: Advances in computational simulation of gravity-induced disproportionate collapse of RC frame buildings. Journal of Structural Engineering, 144(2):03117003, 2018.
[27] Xue, H., Guan, H., Gilbert, B. P., Lu, X., Li, Y.: Simulation of punching and post–punching shear behaviours of RC slab–column connections. Magazine of Concrete Research, 73(22):1135–1150, 2021.
[28] Xue, H., Guan, H., Gilbert, B. P., Lu, X., Li, Y.: Comparative and parametric studies on behavior of RC–flat plates subjected to interior–column Loss. Journal of Structural Engineering, 146(9):04020183, 2020.
[29] Ma, F., Gilbert, B. P., Guan, H., Xue, H., Lu, X., Li, Y.: Experimental study on the progressive collapse behaviour of RC flat plate substructures subjected to corner column removal scenarios. Engineering Structures, 180:728–741, 2019.
[30] Ma, F., Gilbert, B. P., Guan, H., Lu, X., Li, Y.: Experimental study on the progressive collapse behaviour of RC flat plate substructures subjected to edge–column and edge–interior–column removal scenarios. Engineering Structures, 209:110299, 2020.
[31] Xue, H., Gilbert, B. P., Guan, H., Lu, X., Li, Y., Ma, F., Tian, Y.: Load transfer and collapse resistance of RC flat plates under interior column removal scenario. Journal of Structural Engineering, 144(7), 2018.
[32] Brunesi, E., Nascimbene, R., Parisi, F., Augenti, N.: Progressive collapse fragility of reinforced concrete framed structures through incremental dynamic analysis. Engineering Structures, 104:65-79, 2015.
[33] Yang, B., Tan, K. H.: Experimental tests of different types of bolted steel beam–column joints under a central–column–removal scenario. Engineering Structures, 54:112–130, 2013.
[34] Chen, J., Huang, X., Ma, R., He, M.: Experimental study on the progressive collapse resistance of a two–story steel moment frame. Journal of Performance of Constructed Facilities, 26(5):567–575, 2012.
[35] Li, H., Cai, X., Zhang, L., Zhang, B., Wang, W.: Progressive collapse of steel moment-resisting frame subjected to loss of interior column: Experimental tests. Engineering Structures, 150:203–220, 2017.
[36] Tan, Z., Zhong, W. H., Tian, L. M., Zheng, Y. H., Meng, B., Duan, S. C.: Numerical study on collapse-resistant performance of multi-story composite frames under a column removal scenario. Journal of Building Engineering, 44:102957, 2021.
[37] Mucedero, G., Brunesi, E., Parisi, F.: Progressive collapse resistance of framed buildings with partially encased composite beams. Journal of Building Engineering, 38:102228, 2021.
[38] Thelandersson, S., Honfi, D., "Behaviour and modelling of timber structures with reference to robustness," *Proceedings of the Joint Workshop of*

COST Actions TU0601 and E., J. Köhler, H. Narasimhan and M. Faber, eds., 2009.
[39] Masaeli, M., Gilbert, B. P., Karampour, H., Underhill, I. D., Lyu, C. H., Gunalan, S.: Scaling effect on the moment and shear responses of three types of beam–to–column connectors used in mass timber buildings. Engineering Structures, 208:110329, 2020.
[40] Abaqus/CAE, Analysis user's manual version 6.14, 2014.
[41] XLam, Designing with XLam Cross Laminated Timber, *New Zealand Design Guide Version 2.1*, 2016.
[42] Lyu, C. H., Gilbert, B. P., Guan, H., Gunalan, S., Karampour, H.: Finite element modelling of the progressive collapse of post-and-beam mass timber building substructures under edge and corner column removal scenarios. Journal of Building Engineering, 49, 2022.

https://doi.org/10.52202/069179-0368